

A Supersolid Skin Covering both Water and Ice

Xi Zhang^{1,2,a}, Yongli Huang^{3,a}, Zengsheng Ma³, Yichun Zhou^{3,*}, Weitao Zheng⁴, Ji Zhou⁵, and Chang Q Sun^{1-5,*}

¹ *NOVITAS, School of Electrical and Electronic Engineering, Nanyang Technological University, Singapore 639798*

² *Center for Coordination Bond and Electronic Engineering, College of Materials Science and Engineering, China Jiliang University, Hangzhou 310018, China*

³ *Key Laboratory of Low-dimensional Materials and Application Technology (Ministry of Education) and Faculty of Materials, Optoelectronics and Physics, Xiangtan University, Xiangtan, 411105, China*

⁴ *School of Materials Science, Jilin University, Changchun 130012, China*

⁵ *State Key Laboratory of New Ceramics and Fine Processing, Department of Materials Science and Engineering, Tsinghua University, Beijing 100084, China*

^aX.Z. and Y.H. contribute equally.

Contents

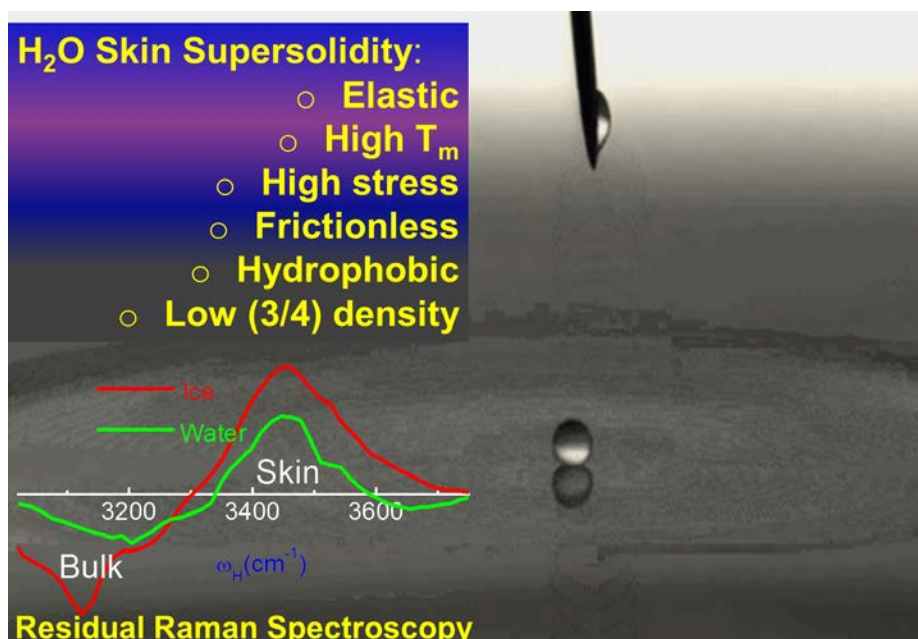
1. Introduction	3
2. Principle: O:H-O bond cooperativity	4
3. Experimental and numerical verification	5
4. Results and discussion.....	6
4.1 Skin-resolved O:H-O bond relaxation	6
4.2 Phonon frequency and thermal stability.....	7
4.3 Skin charge entrapment and polarization-repulsive forces	9
4.4 Stress, viscosity, and elasticity.....	10
5. Summary	11
Acknowledgement.....	12
References:	12

Abstract

The mysterious nature and functionality of water and ice skins remain baffling to the community since 1859 when Faraday firstly proposed liquid skin lubricating ice. Here we show the presence of supersolid phase that covers both water and ice using Raman spectroscopy measurements and quantum calculations. In the skin of two molecular layers thick, molecular undercoordination shortens the H-O bond by ~16% and lengthens the O:H nonbond by ~25% through repulsion between electron pairs on adjacent O atoms, which depresses the density from 0.92 for bulk ice to 0.75 g·cm⁻³. The O:H-O cooperative relaxation stiffens the H-O stretching phonon from 3200/3150 cm⁻¹ to the same value of 3450 cm⁻¹ and raises the melting temperature of both skins by up to ~310 K. Numerical derivatives on the viscoelasticity and charge accumulation suggests that the elastic, polarized, and thermally stable supersolid phase makes the ice frictionless and water skin hydrophobic and ice like at room temperature.

Keywords: Friction, surface tension, hydrogen bond, water, ice, Raman, Density function theory.

TOC entry (see video clip as supporting information)



1. Introduction

Ice skin is most slippery of known¹⁻⁵ and the surface tension of water, 72 dynes/cm at 25 °C⁶, is extraordinarily high. Ice remains slippery while one is standing still on it without even pressure melting or friction heating. Small insects such as a water strider can walk and glide freely on water because: (i) it weighs insufficiently to penetrate the skin and (ii) the interface between its paddle and the skin of water is hydrophobic. If carefully placed on the surface, a small needle floats on the water even though its density is times higher than that of water. If the surface is agitated to break up the tension, then the needle will sink quickly. A high-speed video clip (see Supplementary Information) shows that the repeatedly bouncing of a water droplet on water surface, evidencing that water skin is elastic and hydrophobic.

The high tension and hydrophobicity of water surface was commonly attributed to the presence of a layer of solid ice⁷⁻⁹ while ice slippery was perceived as the presence of a liquid or a quasi-liquid skin serving as the lubricant¹⁰ even at temperature below freezing^{11,12}. Mechanisms of pressure-promoted melting¹³ and friction-induced heating¹⁴ also explained the slippery of ice.

However, the pressure-promoted melting contradicts with the phase diagram of ice below -22 °C, i.e., pressure induces solid-solid transition rather than solid-liquid transition¹⁵, though the pressure could lower the melting point of ice¹³. It is expected that at melting the vibration amplitudes of the surface molecules are folds greater than that in the bulk but an interfacial force microscopy measurements ruled out this prediction². The skin layer is viscoelastic at temperatures ranging from -10 to -30 °C, which evidences the absence of the liquid layer at such low temperatures. The surface pre-melting is also in conflicting with the ice-like nature of ultrathin films of water^{8,9,16}. Vibrational sum frequency spectroscopy measurements and molecular dynamics (MD) calculations suggested that the outermost two layers of water molecules are ordered “ice like” at room temperature^{17,18}, being opposite to the premelting of surface or defect sites demonstrated by other usual materials such as metals¹⁹.

Amazingly, water freezing starts preferentially at sites of molecules with full-coordination neighbors of four. According to MD calculations²⁰, freezing starts firstly in the subsurface of water instead of the top layer that remains disordered during freezing. The bulk melting is mediated by topological defects that preserve the coordination environment of the tetrahedral-coordinated network. Such defects form a region with a longer lifetime than the ideal bulk²¹. Water droplet on roughened Ag surface (with nanocolumnar structures) having a greater contact angle melts 62 sec later than the latter at -4 °C compared with the droplet with smaller contact

angle on a smooth Ag surface²². The critical temperature for transiting the contact the initial contact angle of a droplet to zero is proportional to the its initial value (curvature)²³. Transition happens at 185, 234, and 271 °C for water droplets on quartz, sapphire, and graphite with initial contact angles of 27.9, 64.2, and 84.7°, respectively. These findings indicate that water molecules at highly curved skin are thermally even more stable.

Why is ice so slippery and why is the tension of water skin so high? Does water form skin on ice or the alternative? These questions have baffled the community since 1859 when Farady¹² firstly proposed the presence of a lubricant liquid skin on ice.

We aim to show in this communication that molecular undercoordination induced H-O bond contraction and the O:H nonbond elongation and the associated core electron entrapment and non-bonding lone-pair polarization²⁴⁻²⁶ result in the high-elasticity⁴, self-lubricavity of ice^{1,27} and the hydrophobicity^{16,28} of water and ice skin. Ice slippery results from the lone pair weak yet elastic interaction, which makes the ice self lubricate. The cohesive energy gain of the shortened O-H bond raises the critical temperature of phase transition²⁶, and therefore, a monolayer of water performs like ice at room temperature with high elasticity²⁹ and high core charge density³⁰⁻³². The monolayer skin melts at temperature about 310 K according to the MD derivatives³³.

2 Principle: O:H-O bond cooperativity

Firstly, hydrogen bond (O:H-O) relaxes cooperatively under excitation. The O:H-O bond forms a pair of asymmetric, coupled, H-bridged oscillators with ultra-short interactions^{34,35}. The cooperativity of the O:H-O bond discriminates water ice from other usual materials in the structure order and physical properties. In practice, O atoms always move in the same direction along the O:H-O bond by different amounts²⁶. The softer O:H (d_L length) bond always relaxes more in length than the stiffer H-O (d_H) covalent bond does: $|\Delta d_L| > |\Delta d_H|$. The relaxation in length and energy and the associated local charge distribution of the O:H-O bond determine the anomalies of water ice under various stimuli such as compressing^{26,36,37}, clustering²⁴, and cooling^{25,38}. With the given structure order of tetrahedrally-coordinated molecules and known mass density ρ , one is able to determine the molecular size (d_H , unit in Å), separation (d_{OO} or d_L), of molecules packing in water and ice, in terms of statistic mean³⁴,

$$\begin{cases} d_{oo} = 2.6950\rho^{-1/3} & (\text{Molecular separation}) \\ \frac{d_L}{d_{L0}} = \frac{2}{1 + \exp[(d_H - d_{H0})/0.2428]}; & (d_{H0} = 1.0004 \text{ and } d_{L0} = 1.6946 \text{ at } 4^\circ\text{C}) \end{cases}$$

Secondly, the impact of the O:H-O bond cooperative relaxation is tremendous. The H-O bond contracts and the O:H nonbond expands spontaneously once the molecular coordination number (CN) is reduced from the ideal bulk value of four, which happens in skins defect sites, hydrotion shells, and ultrathin films²⁴. The shortended H-O bond becomes stiffer with a depression of the interatomic potential well, which entraps and densifies the O 1s binding energy^{31,39-41} and local core and bonding charge^{27,32,39,42,43}. The stiffening of the H-O bond raises the critical temperature for phase transition and stiffens the H-O stretching ω_H phonons. Most importantly, the densely entrapped bonding charge polarizes the soluted nonbonding electrons with bound energy (equivalent of work function) changing from 3.2 in the bulk to 1.6 eV in the skin²⁷. The large O:H bond elongation partly compensates for the H-O contraction and partly lengthens the overall O—O distance, resulting in volume expansion⁴⁴⁻⁴⁷. The measured 5.9%~10% skin d_{OO} expansion at the ambient^{34,46} does follow the expectation. Likewise, the 4.0% and 7.5% volume expansion of water molecules confined, respectively, in the 5.1 and 2.8 nm sized hydrophobic TiO₂ pores⁴⁸ provide further evidence for the predicted low density skin.

3. Experimental and numerical verification

In order to verify our predictions, we analyzed the nice set of Raman data collected by Donaldson and co-workers⁴ and conducted quantum calculations using the DFT-derived MD and the dispersion-corrected DFT packages. Calculations was focused on resolving the O:H-O cooperative relaxation in length and stiffness in the skin and the skin charge accumulation. MD calculations were performed using the Forcite code with COMPASS forcefield.⁴⁹ Ice interface is relaxed in NPT ensemble at 180 K for 100 ps to obtain equilibrium. The time step is 0.5 fs. Nose-hoover thermostat with Q ratio of 0.01 is adopted to control the temperature.

Dispersion-corrected DFT structural optimizations of ice surface were performed using Dmol³ code based on the PBE functional⁵⁰ in the general gradient approximation and the dispersion-corrected Tkatchenko-Scheffler scheme⁵¹ with the inclusion of hydrogen bonding and vdW interactions. The all-electron method was used to describe the wave functions with a double numeric and polarization basis sets. The self-consistency threshold of total energy was set at 10^{-6} Hartree. In the structural optimization, the tolerance limits for the energy, force and displacement were set at 10^{-5} Hartree, 0.002 Hartree/Å and 0.005 Å, respectively.

Calculations also extend to examine the charge densification, viscosity, and surface tension at the skin region of 200 K ice. The conventionally used super-cell⁵² as shown in Figure 1 was used in calculations. A vacuum slab is inserted into the super-cell to approximate the liquid-vapor interface or the skin that contains free H-O radicals.

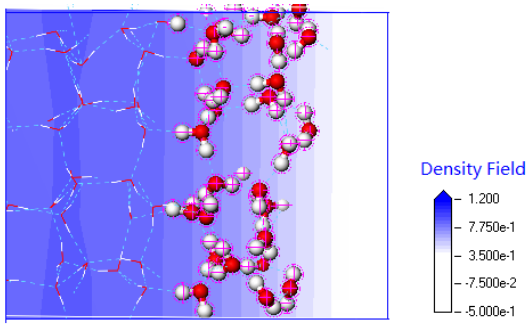


Figure 1 H₂O super-cell with a vacuum slab representing the supersolid skin of ice (200 K) with even undercoordinated H-O radicals with color indicating the MD-derived density field. The current work turns out the skin reduces the H₂O molecular volume but inflates molecular distance because molecular undercoordination shortens and stiffens the d_H and lengthens and polarizes the d_L due to repulsion between the electron pairs on adjacent O atoms and the O:H-O bond mechanical strength disparity.

4. Results and discussion

4.1 Skin-resolved O:H-O bond relaxation

Indeed, the O:H-O bond cooperative relaxation lowers the skin mass density substantially. Figure 2 features the residual length spectra (RLS) for the MD-derived O-H and O:H bond of ice. The RLS is obtained by subtracting the spectrum of a fully-filled unit cell from that containing the vacuum slab. The RLS turns out that the O-H bond contracts from ~ 1.00 in the body to ~ 0.95 at the skin. The O:H elongates from ~ 1.68 in the body to ~ 1.90 Å (average) at the skin, resulting in a 6.8% d_{OO} elongation or a 20% volume expansion. The $d_H = 0.93$ Å peak and the broaden d_L could be reflection of the even undercoordinated H-O radicals that are associated 3650 cm^{-1} vibration frequency²⁴. This result agrees with the trend that the H-O bond contracts from 0.9732 Å at the center to 0.9659 Å at the skin of a water droplet containing 1000 molecules in previous MD calculations⁵³.

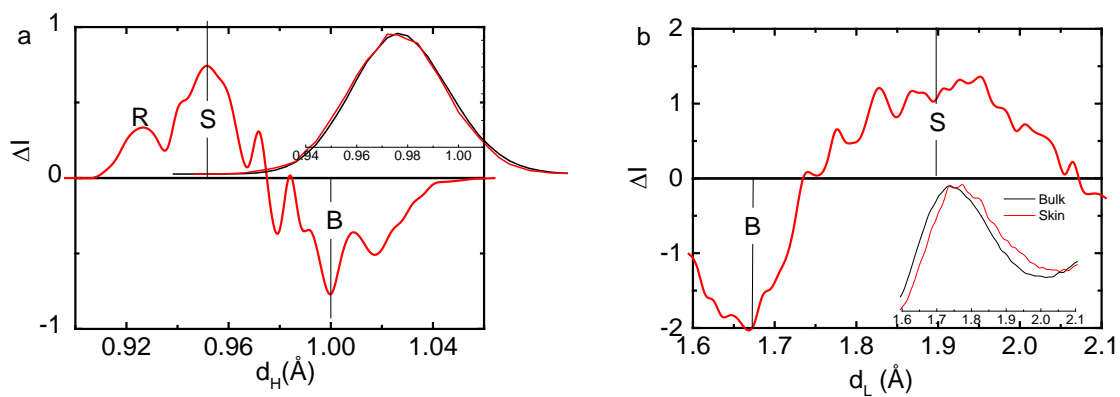


Figure 2 MD-derived RLS of (a) d_H contraction from ~ 1.00 to ~ 0.95 (0.93 for radicals) \AA and (b) d_L elongation from ~ 1.68 to ~ 1.90 \AA (high fluctuation). Insets show the raw data of calculations. R, S and B represent the H-O radicals, skin, and bulk.

Furthermore, the measured $d_{OO} (= 2.965 \text{ \AA})^{46}$ in the water skin turns out, using eq (1), $d_H = 0.8406 \text{ \AA}$ and $d_L = 2.1126 \text{ \AA}$, corresponding to the $0.75 \text{ g}\cdot\text{cm}^{-3}$ mass density that is much lower than the bulk ice of $0.92 \text{ g}\cdot\text{cm}^{-3}$. Therefore, the numerical RLS and the experimental derivatives verified the expectation of the ultra-low density of the skins of both water and ice. Table 1 lists the experimentally-derived bond length (d_{OO} , d_x) and density (ρ) (eq 1), vibration frequency (ω_x), and bond energy (E_x) that was transformed from Lagrangian solution to the O:H-O oscillators with the measured d_{OO} and ω_x as input³⁵. Clearly, skins of water and ice share the same identity of density, bond length, bond strength, vibration frequency, etc., at temperatures of 25 and $-20 \text{ }^\circ\text{C}$.

Table 1 Skin supersolidity (ω_x , d_x , E_x , ρ) of water and ice converted from eq (1) and Lagrangian solution with the known data (indicated with refs) as input based on the water structure^{34,35}. q_H is the effective charge of the proton, which is an adjustable for testing.

	Water (298 K)		Ice (ρ_{\min})		Ice	Vapor
	bulk	skin	bulk		80 K	dimer
$\omega_H(\text{cm}^{-1})$	3200 ⁴	3450 ⁴	3125 ⁴		3090 ²⁵	3650 ⁵⁴
$\omega_L(\text{cm}^{-1})^{25}$	220	$\sim 180^{24}$	210		235	0
$d_{OO}(\text{\AA})^{34}$	2.700 ⁵⁵	2.965 ⁴⁶	2.771		2.751	2.980 ⁴⁶
$d_H(\text{\AA})^{34}$	0.9981	0.8406	0.9676		0.9771	0.8030
$d_L(\text{\AA})^{34}$	1.6969	2.1126	1.8034		1.7739	≥ 2.177
$\rho(\text{g}\cdot\text{cm}^{-3})^{34}$	0.9945	0.7509	0.92 ⁵⁶		0.94 ⁵⁶	≤ 0.7396
$E_L(\text{meV}) \propto (\omega_x \times d_x)^2$	91.6	95 ⁵⁷	94.2		114.2	0
$E_L(\text{meV}) (q_H = 0.20 \text{ e})$	24.6	24.4	26.2		44.3	0
$E_L(\text{meV}) (0.17 \text{ e})$	33.4	33.8	35.1		52.0	0
$*E_H(\text{eV}) (q_H = 0.20 \text{ e})$	3.6201	7.1967	4.0987; 3.97 ²⁵		3.9416	8.6429
$E_H(\text{eV}) (0.10 \text{ e})$	3.6203	7.1968	4.0990		3.9418	8.6429

4.2 Phonon frequency and thermal stability

The supersolid skins of water and ice stiffen the ω_H to the identical frequency of 3450 cm^{-1} and raise the

melting temperature (T_m) substantially. The phonon frequency corresponds to the square root of the stiffness of the specific bond with Y_x being the Young's modulus and the T_m is proportional to the E_H ^{24,35}:

$$\begin{cases} \Delta\omega_x \propto \sqrt{(k_x + k_c) / \mu_x} \propto \sqrt{E_x / \mu_x} / d_x = \sqrt{Y_x d_x / \mu_x} \\ T_m \propto E_H \end{cases} \quad (T_m < T_{evap}) \quad (2)$$

Where k_x and k_c are the force constants, being the 2nd differential of the respective potential (exchange for H-O, van der Waals for O:H, and Coulomb potential for the O—O). The μ_x is the reduced mass of respective H₂O:H₂O (ω_L) and the H-O (ω_H) vibrating dimer.

As demonstrated in²⁴, the temperature of melting is proportional to the H-O bond energy. The stiffening of the H-O bond raises the local freezing/melting temperature accordingly. Therefore, the supersolid skin of water performs like ice at room temperature. This derivative also applies to water droplets encapsulated in hydrophobic nanopores^{29,66,67} and defects elevated local T_m ^{20,21}. According to the E_H derived in Table 1, the skin T_m is twice that of the bulk, but the T_m is subject to the temperature of evaporation T_{evap} that requires energy breaking the H:O bond (0.925 eV⁵⁷). Therefore, the monolayer water melts at temperature about 315 K³³.

Figure 3(a, b) features the calculated residual phonon spectra (RPS) of ω_L and ω_H of ice in comparison to (c) the ω_H measurements from water and ice with insets showing the original raw data⁴. The RPS were obtained by subtracting the spectrum collected at smaller angles (between the surface normal and the reflection beam) from the one collected at larger angles upon the spectral area being normalized. The valleys of the RPS represent the bulk feature while the peaks the skin attributes. Proper offset of the calculated RPS is necessary as the calculation code overestimates the inter- and inter-molecular interactions²⁵.

As expected, the ω_L undergoes a redshift while the ω_H splits into three peaks at the skin. Two ω_H of higher frequencies arise from the undercoordination induced contraction of the bonded (T) and the free H-O radicals (R). The ω_L redshift arises from O-O repulsion and polarization. The polarization in turn screens and splits the interatomic potential, resulting in another ω_H peak (P) below the bulk valley. The R peak corresponds to the even lower-coordinated H-O radicals.

Most strikingly, the measured RPS shows that skins of water and ice share the identical ω_H at 3450 cm⁻¹, which indicates that both skins are the same in nature. This finding agrees with the DFT-MD derivative that the H-O vibration frequency shifts from ~3250 cm⁻¹ at a 7 Å depth to ~3500 cm⁻¹ at the 2 Å skin of water liquid⁵². Therefore, neither ice skin forms on water nor does the otherwise. One can refer such abnormal skins

to the supersolid state. The concept of supersolidity is adopted from the superfluidity of solid ^4He at mK temperatures. The skins of ^4He fragments are highly elastic and frictionless with repulsive force between them at motion⁵⁸.

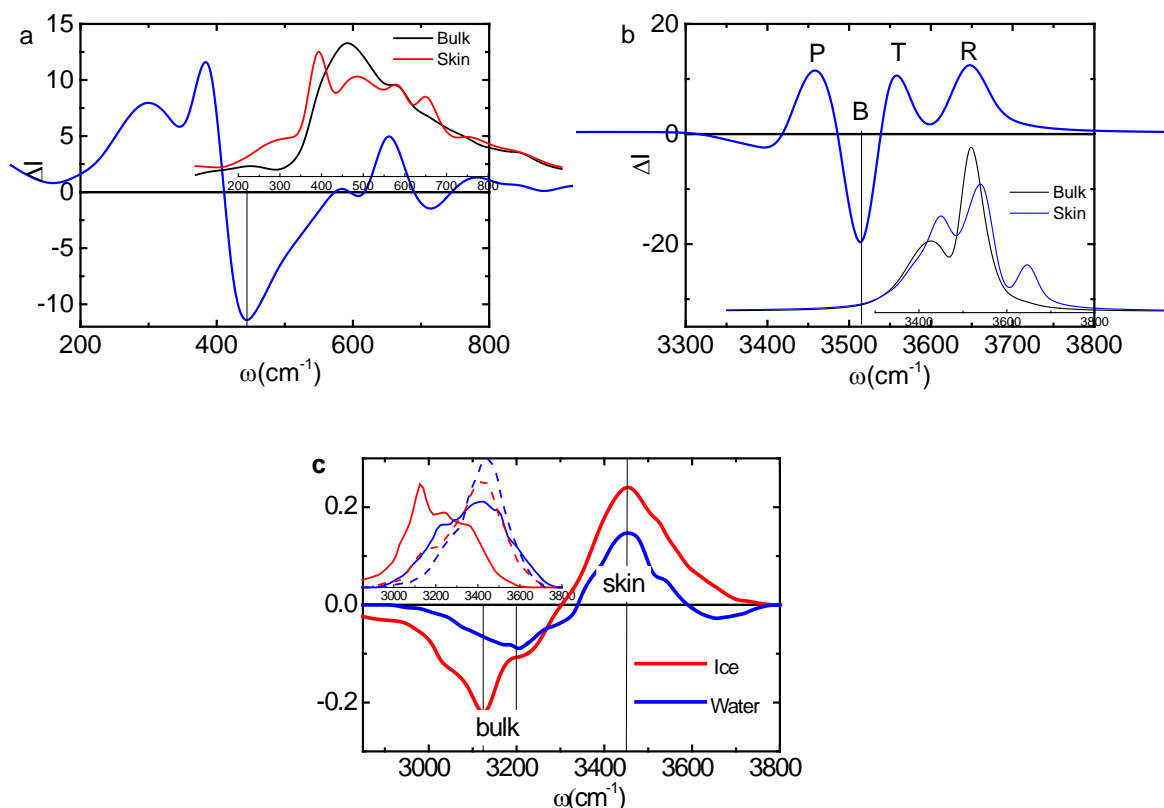


Figure 3 RPS of the MD-derived (a) ω_L and (b) ω_H of ice and (c) the measured ω_H of water (at room-temperature) and ice (at -20 and -15 $^{\circ}\text{C}$)⁴. The ω_L undergoes redshift while the ω_H splits into three. Features T and R correspond to the H-O skin bond and the free H-O radicals and P to the screen and splitting effect on the crystal potentials by the undercoordinated O:H in numerical derivatives. Water and ice skins share the identical ω_H of 3450 cm^{-1} , which clarifies neither liquid skin forms on ice nor solid skin on water.

4.3 Skin charge entrapment and polarization-repulsive forces

The skins do entrap bonding and core electrons, which polarizes nonbonding charge, raises the thermal stability, and creates electronic repulsive force. Table 2 features the DFT-MD derived d_x and the charge polarization at the skin of water. The net charge of a water molecule increases from 0.022 in the body to -0.024 at the skin. As expected, bonding electron gain does happen at the skin. The charge gain and the nonbonding electron polarization provide the sources for the Coulomb repulsive force that reduces the friction at the interface between ice and other materials. Measurements have revealed the presence of the repulsive forces between a hydrated mica-tungsten contacting pair at 24 $^{\circ}\text{C}$ ⁵⁹. Such repulsive interactions appear at

above 20% relative humidity (RH) and are fully developed in the range of 38-45% RH. The repulsion corresponds to an elastic modulus of 6.7 GPa. Monolayer ice also forms on graphite surface at 25% RH and room temperature^{60,61}. These experimental and numerical findings evidence the presence of the supersolidity with repulsive forces as a result of surface polarization and bonding charge accumulation and the elevated melting point resulting due to H-O strength gain.

Table 2 Numerically-derived O:H-O length relaxation, charge densification and polarization at the skin of ice. Negative sign represents net electron gain. MD and DFT show the same trend despite the quantitative discrepancy due to artifacts in calculation approximations.

	Skin		body	
	MD	DFT	MD	DFT
d_H	0.9576	0.9824	1.0002	1.0001
d_L	1.7010	1.7966	1.9195	1.7732
q_o	-	-0.652	-	-0.616
q_H	-	0.314	-	0.319
Net	-	-0.024	-	0.022

4.4 Stress, viscosity, and elasticity

Water and ice skins share high tension and viscosity. The surface tension γ is defined as the difference between the stress components in the direction parallel and perpendicular to the interface^{62,63},

$$\gamma = \frac{1}{2} \left(\frac{\sigma_{xx} + \sigma_{yy}}{2} - \sigma_{zz} \right) \cdot L_z \quad (3)$$

where σ_{xx} , σ_{yy} , and σ_{zz} are the stress tensor element and L_z is the length of the super-cell in the z direction.

Green⁶⁴ and Kubo⁶⁵ correlated the surface shear viscosity η_s to the bulk stress σ in the way:

$$\eta_s = \frac{V}{kT} \int_0^{\infty} \langle \sigma_{\alpha\beta}(0) \sigma_{\alpha\beta}(t) \rangle dt$$

(4)

where the $\sigma_{\alpha\beta}$ denote the three equivalent off-diagonal elements of the stress tensors. The bulk viscosity η_v is related to the decay of fluctuations in the diagonal elements of the stress tensor as follows:

$$\eta_v = \frac{V}{kT} \int_0^{\infty} \langle \delta\sigma(0)\delta\sigma(t) \rangle dt$$

$$\delta\sigma = \sigma - \langle \sigma \rangle$$

(5)

Based on these notations, we calculated the γ using the MD-derived stress tensors. The auto-correlation functions of stress tensors can also be calculated and hence η_s and η_v are obtained according to eq (4) and (5). Table 3 features the MD-derived thickness-dependent γ , η_s , and η_v of ice skin. Reduction of the number of water molecule layers increases the values of γ , η_s , and η_v , which agrees with our expectations. The O:H-O cooperative relaxation and the associated entrapment and polarization enhance the stress tensors to reach the values of 73.6 for 5 layers, approaching the measured 72 dyn/cm at 25 °C.

Table 3 Thickness-dependent surface tension and viscosity of ice skin.

Number-of-layer	15	8	5
γ dyn/cm	31.5	55.2	73.6
η_s	0.0007	0.0012	0.0019
η_v	0.0027	0.0029	0.0032

Skin supersolidity slipperizes ice. The H-O contraction, core electron entrapment and nonbonding electron polarization yield the high-elasticity, self-lubrication, and low-friction of ice and the hydrophobicity of water surface as well. The mechanism of frictionless and self-lubricate of ice⁵ is the same to that of metal nitride surfaces⁶⁶. The friction coefficient of ice and some nitrides are in the same order of 0.1 or below. The elastic recovery coefficient of TiCrN and GaAlN surfaces reaches 100% under a critical indentation load of friction (< 1.0 mN) at which the lone pair breaks. The involvement of lone pairs makes the ice and the nitride skins more elastic and slippery at loads under the critical values.

5 Summary

In summary, experimental and numerical results evidence consistently our skin supersolidity prediction and

the proposed physical origin - O:H-O bond cooperative relaxation and the associated charge entrapment and polarization. Molecular undercoordination shortens and stiffens the H-O bond and meanwhile lengthens and polarizes the O:H bond. In the skin region, molecular becomes smaller but the molecular distance becomes longer and hence the density of the skin drops substantially ($0.75 \text{ g}\cdot\text{cm}^{-3}$). The shortening of the H-O bond raises the density of the core and the bond electrons, which in turn polarize the lone pairs, resulting in the high elasticity and the high density of dipoles. The supersolid skin slipperizes ice and enhances the surface tension of liquid. Neither liquid skin forms on ice nor ice skin forms on water.

Acknowledgement

Financial support received from NSF (Nos.: 21273191, 1033003, and 90922025) China and RG29/12, MOE, Singapore is gratefully acknowledged.

Multimedia movie Available: A high-speed video clip showing the skin supersolidity (elasticity and hydrophobicity) is available free of charge via the Internet at <http://pubs.acs.org>.

Corresponding Author

zhouyc@xtu.edu.cn; ecqsun@ntu.edu.sg; CQ is associated with honorary appointments at the rest affiliations.

References:

- (1) Ishiyama, T.; Takahashi, H.; Morita, A. Origin of Vibrational Spectroscopic Response at Ice Surface. *The Journal of Physical Chemistry Letters* **2012**, *3*, 3001-3006.
- (2) Rosenberg, R. Why Ice Is Slippery? *Phys today* **2005**, 50-55.
- (3) Wei, X.; Miranda, P.; Shen, Y. Surface Vibrational Spectroscopic Study of Surface Melting of Ice. *Physical Review Letters* **2001**, *86*, 1554-1557.
- (4) Kahan, T. F.; Reid, J. P.; Donaldson, D. J. Spectroscopic Probes of the Quasi-Liquid Layer on Ice. *Journal of Physical Chemistry A* **2007**, *111*, 11006-11012.
- (5) Kietzig, A.-M.; Hatzikiriakos, S. G.; Englezos, P. Physics of Ice Friction. *Journal of Applied Physics* **2010**, *107*, 081101-081115.
- (6) Temperature Dependence of Water Surface Tension. <http://Hyperphysics.Phy-Astr.Gsu.Edu/Hbase/Surten.Html#C3>.
- (7) Miranda, P. B.; Xu, L.; Shen, Y. R.; Salmeron, M. Icelike Water Monolayer Adsorbed on Mica at Room Temperature. *Physical Review Letters* **1998**, *81*, 5876-5879.
- (8) McBride, F.; Darling, G. R.; Pussi, K.; Hodgson, A. Tailoring the Structure of Water at a Metal Surface: A Structural Analysis of the Water Bilayer Formed on an Alloy Template. *Physical Review Letters* **2011**, *106*, 226101.
- (9) Michaelides, A.; Morgenstern, K. Ice Nanoclusters at Hydrophobic Metal Surfaces. *Nat. Mater.* **2007**, *6*,

597-601.

(10) Furukawa, Y.; Yamamoto, M.; Kuroda, T. Ellipsometric Study of the Transition Layer on the Surface of an Ice Crystal. *Journal of Crystal Growth* **1987**, *82*, 665-677.

(11) Ryzhkin, I. A.; Petrenko, V. F. Quasi-Liquid Layer Theory Based on the Bulk First-Order Phase Transition. *Journal of Experimental and Theoretical Physics* **2009**, *108*, 68-71.

(12) Faraday, M. *Experimental Researches in Chemical and Physics*; Taylor and Francis London, 1859.

(13) Thomson, J. Theoretical Considerations on the Effect of Pressure in Lowering the Freezing Point of Water. *Cambridge and Dublin Mathematical Journal* **1850**, *11*, 248-255.

(14) Bowden, F. P.; Hughes, T. P. The Mechanism of Sliding on Ice and Snow. *Proc. R. Soc. London* **1939**, *A172*, 280.

(15) Colbeck, S. C.; Najarian, L.; Smith, H. B. Sliding Temperatures of Ice Skates *Am. J. Phys.* **1997**, *65*, 488.

(16) Wang, C.; Lu, H.; Wang, Z.; Xiu, P.; Zhou, B.; Zuo, G.; Wan, R.; Hu, J.; Fang, H. Stable Liquid Water Droplet on a Water Monolayer Formed at Room Temperature on Ionic Model Substrates. *Physical Review Letters* **2009**, *103*, 137801-137804.

(17) Fan, Y. B.; Chen, X.; Yang, L. J.; Cremer, P. S.; Gao, Y. Q. On the Structure of Water at the Aqueous/Air Interface. *Journal of Physical Chemistry B* **2009**, *113*, 11672-11679.

(18) Tainter, C. J.; Ni, Y.; Shi, L.; Skinner, J. L. Hydrogen Bonding and Oh-Stretch Spectroscopy in Water: Hexamer (Cage), Liquid Surface, Liquid, and Ice. *The Journal of Physical Chemistry Letters* **2012**, *4*, 12-17.

(19) Sun, C. Q. *Relaxation of the Chemical Bond*; ISBN: 978-981-4585-20-0; Berlin, 2014 Vol. 108.

(20) Vrbka, L.; Jungwirth, P. Homogeneous Freezing of Water Starts in the Subsurface. *Journal of Physical Chemistry B* **2006**, *110*, 18126-18129.

(21) Donadio, D.; Raiteri, P.; Parrinello, M. Topological Defects and Bulk Melting of Hexagonal Ice. *Journal of Physical Chemistry B* **2005**, *109*, 5421-5424.

(22) Singh, D. P.; Singh, J. P. Delayed Freezing of Water Droplet on Silver Nanocolumnar Thin Film. *Applied Physics Letters* **2013**, *102*, 243112.

(23) Friedman, S. R.; Khalil, M.; Taborak, P. Wetting Transition in Water. *Physical Review Letters* **2013**, *111*.

(24) Sun, C. Q.; Zhang, X.; Zhou, J.; Huang, Y.; Zhou, Y.; Zheng, W. Density, Elasticity, and Stability Anomalies of Water Molecules with Fewer Than Four Neighbors. *The Journal of Physical Chemistry Letters* **2013**, *4*, 2565-2570.

(25) Sun, C. Q.; Zhang, X.; Fu, X.; Zheng, W.; Kuo, J.-I.; Zhou, Y.; Shen, Z.; Zhou, J. Density and Phonon-Stiffness Anomalies of Water and Ice in the Full Temperature Range. *Journal of Physical Chemistry Letters* **2013**, *4*, 3238-3244.

(26) Sun, C. Q.; Zhang, X.; Zheng, W. T. Hidden Force Opposing Ice Compression. *Chem Sci* **2012**, *3*, 1455-1460.

(27) Siefertmann, K. R.; Liu, Y.; Lugovoy, E.; Link, O.; Faubel, M.; Buck, U.; Winter, B.; Abel, B. Binding Energies, Lifetimes and Implications of Bulk and Interface Solvated Electrons in Water. *Nature Chemistry* **2010**, *2*, 274-279.

(28) James, M.; Darwish, T. A.; Ciampi, S.; Sylvester, S. O.; Zhang, Z. M.; Ng, A.; Gooding, J. J.; Hanley, T. L. Nanoscale Condensation of Water on Self-Assembled Monolayers. *Soft Matter* **2011**, *7*, 5309-5318.

(29) Wren, S. N.; Donaldson, D. J. Exclusion of Nitrate to the Air-Ice Interface During Freezing. *The Journal of Physical Chemistry Letters* **2011**, *2*, 1967-1971.

(30) Winter, B.; Aziz, E. F.; Hergenroth, U.; Faubel, M.; Hertel, I. V. Hydrogen Bonds in Liquid Water Studied by Photoelectron Spectroscopy. *Journal of Chemical Physics* **2007**, *126*, 124504.

(31) Vacha, R.; Marsalek, O.; Willard, A. P.; Bonthuis, D. J.; Netz, R. R.; Jungwirth, P. Charge Transfer between Water Molecules as the Possible Origin of the Observed Charging at the Surface of Pure Water. *Journal of Physical Chemistry Letters* **2012**, *3*, 107-111.

(32) Liu, S.; Luo, J.; Xie, G.; Guo, D. Effect of Surface Charge on Water Film Nanoconfined between Hydrophilic Solid Surfaces. *Journal of Applied Physics* **2009**, *105*, 124301-124304.

- (33) Qiu, H.; Guo, W. Electromelting of Confined Monolayer Ice. *Physical Review Letters* **2013**, *110*, 195701.
- (34) Huang, Y.; Zhang, X.; Ma, Z.; Zhou, Y.; Zhou, J.; Zheng, W.; Sun, C. Q. Size, Separation, Structure Order, and Mass Density of Molecules Packing in Water and Ice. *Scientific Reports* **2013**, *3*, 3005.
- (35) Huang, Y.; Zhang, X.; Ma, Z.; Zhou, Y.; Zhou, G.; Sun, C. Q. Hydrogen-Bond Asymmetric Local Potentials in Compressed Ice. *Journal of Physical Chemistry B* **2013**, *117*, 13639-13645.
- (36) Tian, L.; Kolesnikov, A. I.; Li, J. Ab Initio Simulation of Hydrogen Bonding in Ices under Ultra-High Pressure. *The Journal of Chemical Physics* **2012**, *137*, -.
- (37) Yim, W.-L.; Tse, J. S.; Iitaka, T. Pressure-Induced Intermolecular Interactions in Crystalline Silane-Hydrogen. *Physical Review Letters* **2010**, *105*, 215501.
- (38) Medcraft, C.; McNaughton, D.; Thompson, C. D.; Appadoo, D. R. T.; Bauerecker, S.; Robertson, E. G. Water Ice Nanoparticles: Size and Temperature Effects on the Mid-Infrared Spectrum. *Physical Chemistry Chemical Physics* **2013**, *15*, 3630-3639.
- (39) Marsalek, O.; Uhlig, F.; Frigato, T.; Schmidt, B.; Jungwirth, P. Dynamics of Electron Localization in Warm Versus Cold Water Clusters. *Physical Review Letters* **2010**, *105*, 043002.
- (40) Turi, L.; Sheu, W. S.; Rosky, P. J. Characterization of Excess Electrons in Water-Cluster Anions by Quantum Simulations. *Science* **2005**, *309*, 914-917.
- (41) Baletto, F.; Cavazzoni, C.; Scandolo, S. Surface Trapped Excess Electrons on Ice. *Physical Review Letters* **2005**, *95*, 176801.
- (42) Paik, D. H.; Lee, I. R.; Yang, D. S.; Baskin, J. S.; Zewail, A. H. Electrons in Finite-Sized Water Cavities: Hydration Dynamics Observed in Real Time. *Science* **2004**, *306*, 672-675.
- (43) Verlet, J. R. R.; Bragg, A. E.; Kammrath, A.; Cheshnovsky, O.; Neumark, D. M. Observation of Large Water-Cluster Anions with Surface-Bound Excess Electrons. *Science* **2005**, *307*, 93-96.
- (44) Abu-Samha, M.; Borve, K. J. Surface Relaxation in Water Clusters: Evidence from Theoretical Analysis of the Oxygen 1s Photoelectron Spectrum. *Journal of Chemical Physics* **2008**, *128*, 154710.
- (45) Liu, K.; Cruzan, J. D.; Saykally, R. J. Water Clusters. *Science* **1996**, *271*, 929-933.
- (46) Wilson, K. R.; Schaller, R. D.; Co, D. T.; Saykally, R. J.; Rude, B. S.; Catalano, T.; Bozek, J. D. Surface Relaxation in Liquid Water and Methanol Studied by X-Ray Absorption Spectroscopy. *Journal of Chemical Physics* **2002**, *117*, 7738-7744.
- (47) Lenz, A.; Ojamae, L. A Theoretical Study of Water Equilibria: The Cluster Distribution Versus Temperature and Pressure for (H₂O)(N), N=1-60, and Ice. *Journal of Chemical Physics* **2009**, *131*, 134302.
- (48) Solveyra, E. G.; de la Llave, E.; Molinero, V.; Soler-Illia, G.; Scherlis, D. A. Structure, Dynamics, and Phase Behavior of Water in TiO₂ Nanopores. *Journal of Physical Chemistry C* **2013**, *117*, 3330-3342.
- (49) Sun, H. Compass: An Ab Initio Forcefield Optimized for Condensed-Phase Applications - Overview with Details on Alkane and Benzene Compounds. *J. Phys. Chem. B* **1998**, *102*, 7338.
- (50) Perdew, J. P.; Burke, K.; Ernzerhof, M. *Phys. Rev. Lett.* **1996**, *77*, 3865
- (51) Tkatchenko, A.; Scheffler, M. Accurate Molecular Van Der Waals Interactions from Ground-State Electron Density and Free-Atom Reference Data. *Phys. Rev. Lett.* **2009**, *102*, 073005
- (52) Sulpizi, M.; Salanne, M.; Sprik, M.; Gageot, M.-P. Vibrational Sum Frequency Generation Spectroscopy of the Water Liquid-Vapor Interface from Density Functional Theory-Based Molecular Dynamics Simulations. *J. Phys. Chem. Lett.* **2012**, *4*, 83-87.
- (53) Townsend, R. M.; Rice, S. A. Molecular Dynamics Studies of the Liquid-Vapor Interface of Water. *J. Chem. Phys.* **1991**, *94*, 2207-2218.
- (54) Shen, Y. R.; Ostroverkhov, V. Sum-Frequency Vibrational Spectroscopy on Water Interfaces: Polar Orientation of Water Molecules at Interfaces. *Chem Rev* **2006**, *106*, 1140-1154.

- (55) Bergmann, U.; Di Cicco, A.; Wernet, P.; Principi, E.; Glatzel, P.; Nilsson, A. Nearest-Neighbor Oxygen Distances in Liquid Water and Ice Observed by X-Ray Raman Based Extended X-Ray Absorption Fine Structure. *The Journal of Chemical Physics* **2007**, *127*, 174504.
- (56) Mallamace, F.; Broccio, M.; Corsaro, C.; Faraone, A.; Majolino, D.; Venuti, V.; Liu, L.; Mou, C. Y.; Chen, S. H. Evidence of the Existence of the Low-Density Liquid Phase in Supercooled, Confined Water. *Proceedings of the National Academy of Sciences of the United States of America* **2007**, *104*, 424-428.
- (57) Zhao, M.; Zheng, W. T.; Li, J. C.; Wen, Z.; Gu, M. X.; Sun, C. Q. Atomistic Origin, Temperature Dependence, and Responsibilities of Surface Energetics: An Extended Broken-Bond Rule. *Physical Review B* **2007**, *75*, 085427.
- (58) Sun, C. Q.; Sun, Y.; Ni, Y. G.; Zhang, X.; Pan, J. S.; Wang, X. H.; Zhou, J.; Li, L. T.; Zheng, W. T.; Yu, S. S. Coulomb Repulsion at the Nanometer-Sized Contact: A Force Driving Superhydrophobicity, Superfluidity, Superlubricity, and Supersolidity. *Journal of Physical Chemistry C* **2009**, *113*, 20009-20019.
- (59) Xu, D.; Liechti, K. M.; Ravi-Chandar, K. Mechanical Probing of Icelike Water Monolayers. *Langmuir* **2009**, *25*, 12870-12873.
- (60) Jinesh, K. B.; Frenken, J. W. M. Experimental Evidence for Ice Formation at Room Temperature. *Physical Review Letters* **2008**, *101*, 036101.
- (61) Jinesh, K. B.; Frenken, J. W. M. Capillary Condensation in Atomic Scale Friction: How Water Acts Like a Glue. *Physical Review Letters* **2006**, *96*, 166103.
- (62) Dang, L. X.; Chang, T.-M. Molecular Dynamics Study of Water Clusters, Liquid, and Liquid-Vapor Interface of Water with Many-Body Potentials. *The Journal of Chemical Physics* **1997**, *106*, 8149-8159.
- (63) Nijmeijer, M. J. P.; Bakker, A. F.; Bruin, C.; Sikkenk, J. H. A Molecular Dynamics Simulation of the Lennard - Jones Liquid-Vapor Interface. *The Journal of Chemical Physics* **1988**, *89*, 3789-3792.
- (64) Green, M. S. Markoff Random Processes and the Statistical Mechanics of Time - Dependent Phenomena *J. Chem. Phys.* **1952**, *20*, 1281.
- (65) Kubo, R. Statistical Mechanical Theory of Irreversible Processes. I. General Theory and Simple Applications to Magnetic and Conduction Problems. *J. Phys. Soc. Jpn.* **1957**, *12*, 570.
- (66) Sun, C. Q. Thermo-Mechanical Behavior of Low-Dimensional Systems: The Local Bond Average Approach. *Progress in Materials Science* **2009**, *54*, 179-307.